Effect of Supplementary Cementitious Materials on Corrosion Resistance of Reinforced Concrete

By: **Jasim Mohammed Abed**

Corresponding author email: jasimabd@ntu.edu.iq

Abstract: Reinforced concrete (RC) is fundamental to contemporary infrastructure; yet, its longevity is significantly undermined by the corrosion of steel reinforcement, especially in environments rich in chlorides and sulfates. This research examines the synergistic impacts of Supplementary Cementitious Materials (SCMs)—fly ash (FA), silica fume (SF), ground granulated blast furnace slag (GGBS), and metakaolin (MK)—on corrosion resistance, strength progression, and durability improvement. An extensive experimental program was executed, including chloride diffusion tests, sulfate resistance evaluations, and electrochemical corrosion assessments. The findings indicated that multi-SCM blends much surpassed individual replacements, decreasing chloride permeability by 68%, sulfate-induced expansion by 64%, and steel mass loss by 81% relative to conventional concrete. The optimal mix (M13) demonstrated enhanced microstructural refinement, attaining a compressive strength of 70.7 MPa (38% more than the control mix) while preserving remarkable resistance to hostile ions. Nonetheless, increased SCM content adversely impacted workability, resulting in slump values decreasing by as much as 38%. Although superplasticizers alleviated this problem, practical obstacles persist for large-scale implementations. Additionally, the long-term performance under actual exposure settings needs additional investigation to corroborate the laboratory results. This study underscores the significant potential of SCMs in prolonging the service life of concrete, especially in adverse situations. Subsequent research should concentrate on refining mix designs, improving field applicability, and investigating hybrid durability solutions. The results facilitate the development of sustainable, high-performance concrete with improved corrosion resistance and durability, advancing the next generation of resilient infrastructure.

Keywords: synergistic effects, supplementary cementitious materials, corrosion resistance, mechanical properties.

1. Introduction

Reinforced concrete (RC) serves as the foundation of contemporary infrastructure, extensively used in edifices, bridges, and maritime constructions owing to its exceptional mechanical qualities and economic efficiency. Nonetheless, a fundamental constraint is the corrosion of embedded steel reinforcement, which markedly diminishes the durability and service life of concrete buildings. Corrosion-induced degradation results in spalling, cracking, and loss of strength, hence escalating maintenance costs and compromising structural integrity. In hostile conditions, such as coastal areas and industrial sites, the infiltration of chlorides (Cl^-), sulfates (SO_4^{2-}), and carbonation hastens steel corrosion, making corrosion resistance an essential factor in concrete construction [1]–[3]. The integration of Supplementary Cementitious Materials (SCMs) has garnered considerable focus in recent studies to alleviate corrosion hazards. Supplementary cementitious materials (SCMs) including fly ash (FA), silica fume (SF), ground granulated blast furnace slag (GGBS), and metakaolin (MK) are used as partial substitutes for cement to augment durability, diminish permeability, and boost concrete's resistance to hostile ions. [4]–[6]. These materials demonstrate pozzolanic and cementitious reactions, enhancing the microstructure of concrete and reducing the penetration of corrosive chemicals [7]. The corrosion of steel inside concrete is an electrochemical phenomenon that transpires in the presence of oxygen and moisture. The principal mechanisms comprise:

1. Chloride-Induced Corrosion: Chloride ions infiltrate the concrete, disrupting the passive oxide layer on steel, resulting in localized pitting corrosion [8].
2. Sulfate Attack: Sulfates interact with hydrated cement phases, resulting in the formation of expansive compounds (e.g., ettringite), which causes cracking and heightened permeability [9].
3. Carbonation-Induced Corrosion: The interaction between CO_2 and calcium hydroxide diminishes concrete alkalinity, resulting in steel depassivation and uniform corrosion [10].

SCMs diminish porosity, enhance the pore architecture, and sequester chloride ions, thereby postponing corrosion onset and mitigating its propagation rate [11]. The degree of enhancement is contingent upon the kind, replacement level, and mix of supplementary cementitious materials used [12]. SCMs enhance corrosion resistance via many mechanisms:

- Fly Ash (FA) improves sulfate resistance and diminishes chloride penetration by occupying micro-voids and optimizing pore connectivity. Replacement values of 10%–30% provide substantial improvements in corrosion resistance [13].
- Silica Fume (SF): SF is particularly efficient in diminishing permeability owing to its ultrafine particle size and elevated pozzolanic activity. Silica fume at 10%–20% substitution significantly decreases chloride diffusion [14].
- Ground Granulated Blast Furnace Slag (GGBS) improves durability by decreasing calcium hydroxide levels, enhancing sulfate resistance, and optimizing pore structure. The ideal replacement amounts vary from 10% to 35% [15].
- Metakaolin (MK) raises concrete density, improves sulfate resistance, and diminishes capillary porosity, with optimal replacement levels ranging from 5% to 15% [16].

Recent studies demonstrate that the amalgamation of many SCMs may have a synergistic impact, resulting in enhanced corrosion resistance relative to singular alternatives [17]. The ideal mix proportions and interactions among SCMs continue to be a topic of active investigation. Although several studies have examined the impacts of individual SCMs, there is a paucity of literature systematically analyzing their collective impact on corrosion resistance. Furthermore, the enduring performance of multi-SCM concrete in extremely demanding situations remains little investigated [18].

This research seeks to examine the synergistic effects of FA, SF, GGBS, and MK on corrosion resistance. Determine the ideal mixture ratios to enhance durability and corrosion resistance. Assess the impact of supplementary cementitious materials on chloride and sulfate resistance. Examine microstructural changes in SCM-modified concrete.

2. Materials

2.1. Cement: In this particular investigation, ordinary Portland cement (OPC) of Type I was used. In order to supply concrete with the early strength and hydration products that were required, OPC was used. Table 1 provides the details of the chemical composition of OPC as well as its physical characteristics.

Table 1: Chemical and Physical Properties of OPC

Property	Value	Test Standard
Specific Gravity	3.13	ASTM C188 [18]
Fineness (Blaine) (m^2/kg)	329	ASTM C204 [19]
Initial Setting Time (min)	115	ASTM C191 [20]
Final Setting Time (min)	385	ASTM C191 [20]
Compressive Strength (MPa, 28 days)	45.8	ASTM C109 [21]
SiO_2 (%)	22.7	ASTM C114 [22]
Al_2O_3 (%)	6.1	ASTM C114 [22]
Fe_2O_3 (%)	4.3	ASTM C114 [22]
CaO (%)	62.6	ASTM C114 [22]
MgO (%)	3.3	ASTM C114 [22]

2.2. Fly Ash (FA): Class F Fly Ash was used as a pozzolanic additive, substituting 10%, 20%, and 30% of cement. It facilitated the reduction of permeability, the refinement of pore structure, and the enhancement of sulfate resistance. The physical and chemical characteristics of Fly Ash are delineated in Table 2.

Table 2: Chemical and Physical Properties of Fly Ash

Property	Value	Test Standard
Specific Gravity	2.31	ASTM C188 [18]
Fineness (Retained on 45 μm, %)	20	ASTM C430 [24]
Pozzolanic Activity (MPa, 28 days)	33	ASTM C311 [25]
SiO_2 (%)	52.5	ASTM C618 [26]
Al_2O_3 (%)	27.1	ASTM C618 [26]
Fe_2O_3 (%)	10.2	ASTM C618 [26]

Property	Value	Test Standard
CaO (%)	5.1	ASTM C618 [26]

2.3. Silica Fume (SF): Silica fume was used at replacement levels of 10% and 20%. Its ultrafine particle size markedly decreased permeability and enhanced the density of concrete. The physical and chemical characteristics of Silica Fume are delineated in Table 3.

Table 3: Chemical and Physical Properties of Silica Fume

Property	Value	Test Standard
Specific Gravity	2.32	ASTM C1240 [27]
Mean Particle Size (μm)	0.16	ASTM C1240 [27]
Specific Surface Area (m^2/g)	18	ASTM C1240 [27]
SiO_2 (%)	90.7	ASTM C618 [26]
Al_2O_3 (%)	0.55	ASTM C618 [26]
Fe_2O_3 (%)	0.32	ASTM C618 [26]
Loss on Ignition (%)	3.1	ASTM C618 [26]

2.4. Ground Granulated Blast Furnace Slag (GGBS): Improvements in sulfate resistance, reduction in heat of hydration, and refinement of pore structure were achieved with the incorporation of GGBS at replacement levels of 10%, 20%, and 35% respectively. The following table provides a listing of the physical and chemical parameters of the GGBS that was employed.

Table 4: Chemical and Physical Properties of GGBS

Property	Value	Test Standard
Specific Gravity	2.58	ASTM C188 [18]
Fineness (Blaine) (m^2/kg)	290	ASTM C204 [19]
SiO_2 (%)	36.7	ASTM C989 [28]
Al_2O_3 (%)	15.8	ASTM C989 [28]
Fe_2O_3 (%)	0.66	ASTM C989 [28]
CaO (%)	44.7	ASTM C989 [28]
MgO (%)	6.5	ASTM C989 [28]

2.5. Metakaolin (MK): Increased early-age strength, decreased porosity, and enhanced resilience to harsh conditions were all achieved with the use of metakaolin at replacement levels of 5%, 10%, and 15% respectively. The following table provides a listing of the physical and chemical characteristics of the Metakaolin powder that was employed.

Table 5: Chemical and Physical Properties of Metakaolin

Property	Value	Test Standard
Specific Gravity	2.45	ASTM C188 [18]

Property	Value	Test Standard
Median Particle Size (μm)	2.65	ASTM C618 [26]
SiO_2 (%)	53.5	ASTM C618 [26]
Al_2O_3 (%)	43.7	ASTM C618 [26]
Fe_2O_3 (%)	1.22	ASTM C618 [26]
Loss on Ignition (%)	0.62	ASTM C618 [26]

This research replicated a very hostile environment using a mixed sulfate and chloride solution to assess the corrosion resistance of reinforced concrete. The exposure solution included sodium sulfate (Na_2SO_4), magnesium sulfate ($MgSO_4$), and sodium chloride (NaCl) with a total molarity of 0.35 M. These chemicals were chosen because of their common occurrence in maritime environments, industrial settings, and sulfate-rich soils that exacerbate reinforcement corrosion and concrete degradation.

2.6. Sodium Sulfate (Na_2SO_4): Sodium sulfate (Na_2SO_4) was added to the test solution to replicate sulfate assault, which may result in expansion, cracking, and deterioration of concrete durability. The interaction of sulfate ions (SO_4^{2-}) with calcium hydroxide ($Ca(OH)_2$) and calcium aluminate hydrates (C-A-H) in concrete leads to the production of gypsum ($CaSO_4 \cdot 2H_2O$) and ettringite ($Ca_6Al_2(SO_4)_3(OH)_{12} \cdot 26H_2O$), both of which induce microstructural deterioration and compromise the integrity of concrete. The physical and chemical parameters of sodium sulfate (Na_2SO_4) are shown in Table 6 below.

Table 6: Physical and Chemical Properties of Sodium Sulfate (Na_2SO_4)

Property	Value	Test Standard
Molecular Weight (g/mol)	143.11	ASTM D516 [30]
Solubility in Water (g/L at 20°C)	48.3	
pH (1% solution)	6.5	
Appearance	Crystalline white powder	
Anion Present	SO_4^{2-}	

2.7. Magnesium Sulfate ($MgSO_4$): Magnesium sulfate ($MgSO_4$) was included into the test solution to replicate the synergistic impact of sulfate assault and magnesium infiltration. In contrast to sodium sulfate, Mg^{2+} ions interact with calcium silicate hydrates (C-S-H), resulting in their disintegration and substitution with non-cementitious magnesium silicate hydrates (M-S-H), hence diminishing the mechanical qualities of concrete. Nevertheless, the physical and chemical characteristics of magnesium sulfate ($MgSO_4$) are shown in Table 7 below.

Table 7: Physical and Chemical Properties of Magnesium Sulfate ($MgSO_4$)

Property	Value	Test Standard
Molecular Weight (g/mol)	121.45	ASTM C1012 [31]
Solubility in Water (g/L at 20°C)	71.2	
pH (1% solution)	6	
Appearance	Crystalline white powder	

Property	Value	Test Standard
Anion Present	SO_4^{2-}	

2.8. Sodium Chloride (NaCl): Sodium chloride (NaCl) was included into the exposure solution to replicate chloride-induced corrosion, the predominant cause of reinforcement corrosion in concrete buildings. Chloride ions infiltrate the concrete matrix, disrupting the protective passive layer on the reinforcing steel and instigating pitting corrosion, which considerably diminishes the structural integrity of reinforced concrete. The physical and chemical characteristics of Sodium Chloride (NaCl) are shown in Table 8 below.

Table 8: Physical and Chemical Properties of Sodium Chloride (NaCl)

Property	Value	Test Standard
Molecular Weight (g/mol)	59.55	ASTM D512 [32]
Solubility in Water (g/L at 20°C)	361	
pH (1% solution)	7.1	
Appearance	Crystalline white powder	
Anion Present	Cl^-	

2.9. Exposure Solution Composition: The exposure solution was formulated by dissolving sodium sulfate (Na_2SO_4), magnesium sulfate ($MgSO_4$), and sodium chloride (NaCl) in distilled water to attain a total molarity of 0.35 M. The specific molarities of each chemical were modified according to the environmental exposure circumstances present in marine, sulfate-rich soils, and industrial areas. The chemical composition of the Aggressive Exposure Solution is shown in Table 9.

Table 9: Composition of the Aggressive Exposure Solution

Chemical Compound	Molarity (M)	Mass per Liter (g/L)
Na_2SO_4	0.11	14.1
$MgSO_4$	0.12	12.2
NaCl	0.16	8.7
Total Molarity	0.37	35.2

2.10. Steel bars: Reinforcing steel bars were manufactured in accordance with the ASTM A615/A615M-20 standard, which ensured that they had constant chemical and mechanical qualities that were acceptable for structural purposes. In order to provide acceptable load-carrying capacity and resistance to plastic deformation, high yield strength (432 MPa) is considered necessary. Additionally, extra safety margins before failure are provided by the Ultimate Tensile Strength, which is 642 MPa. By increasing the steel's ductility by 10.2%, the elongation capacity makes it possible for the steel to withstand deformation without experiencing an abrupt failure.

3. Test procedure and research methodology

As can be seen in Fig. 1, a thorough experimental program was created in order to examine the synergistic effects of SCMs on corrosion resistance. These SCMs include fly ash (FA), silica fume (SF), ground granulated blast furnace slag (GGBS), and metakaolin (MK). In the course of the study,

3.1. Slump Test

In order to determine the degree to which each concrete mixture was workable, the slump test according to ASTM C143[33] was carried out. In this experiment, a typical Abrams cone was used, and the height of the droop was measured immediately after the cone was lifted. For the purpose of determining the impact that SCMs and chemical admixtures have on flowability, this test was absolutely necessary.

3.2. Compressive Strength Test

After a period of ninety days, the compressive strength of concrete cylinders measuring 100 mm × 200 mm was evaluated according to ASTM.C39[34]. With the use of a hydraulic compression testing equipment, the specimens were loaded axially until they broke without breaking. In particular, the results of this test shed light on the impact that SCMs have on the development of strength, especially in settings including sulfate and chloride.

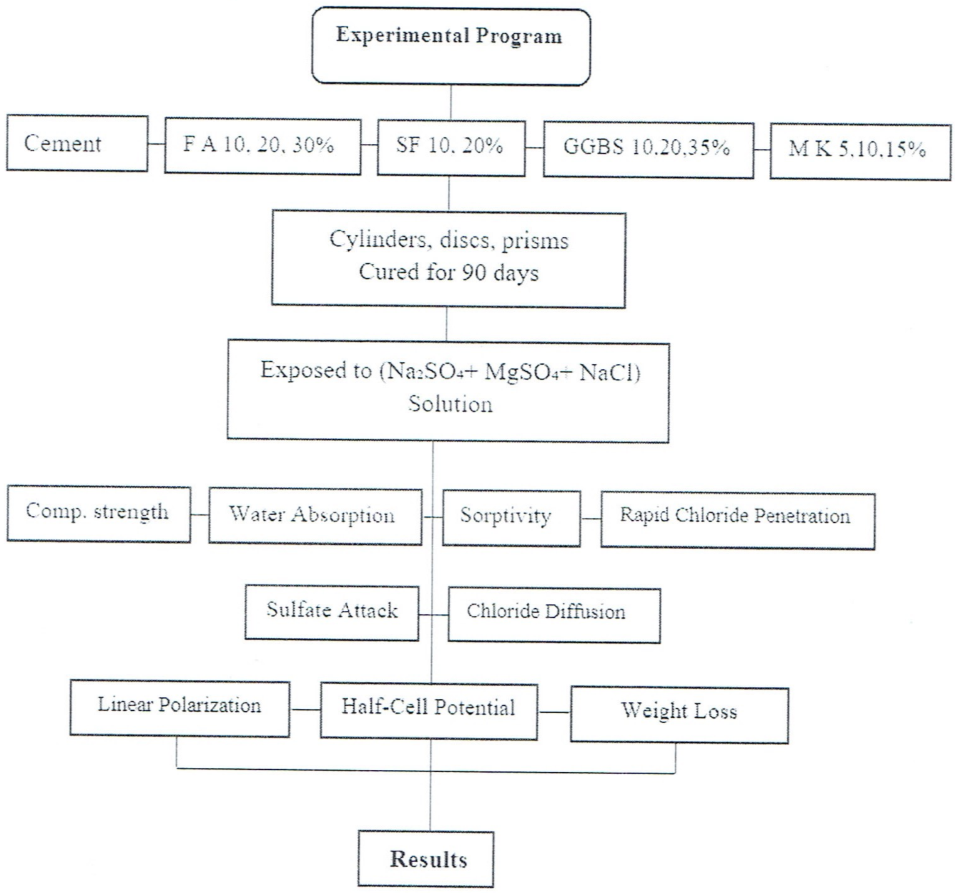

Fig. 1. Schematic diagram of research methodology

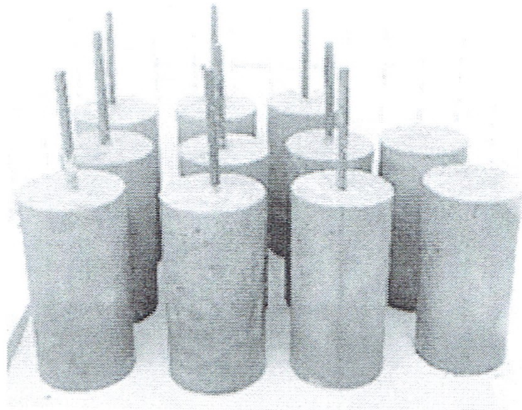

Fig.2. Compressive strength of concrete cylinders

3.3. Water Absorption and Sorptivity Tests

For the purpose of determining water absorption according to ASTM C642[35], concrete samples were dried in an oven, then submerged in water, and the weight changes were recorded. Sorptivity ASTM C1585[36] evaluated the rate of capillary absorption, which indicated the refinement of the pore structure that was caused by SCMs because of their presence. Both of these tests were essential in order to evaluate the permeability properties of SCM-modified concrete as well as its capacity to withstand the infiltration of chloride and sulfate.

3.4. Rapid Chloride Penetration Test (RCPT)

Figure 3 depicts the results of the RCPT ASTM C1202[37] test that was carried out in order to determine the chloride ion permeability of concrete. The specimens, which were in the form of discs and were 100 millimeters by 50 millimeters, were positioned in a two-cell system, with a solution of sodium chloride on one side and a solution of sodium hydroxide on the other. For a period of six hours, a potential of sixty volts was applied, and the total charge that was passed (in Coulombs) was measured. It was determined that lower charge values suggested a stronger resistance to chloride penetration, which is an essential component of corrosion resistance.

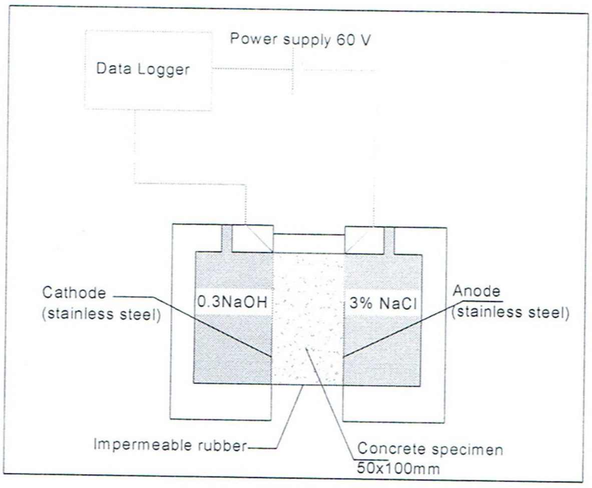

Fig. 3 Chloride Penetration Tests

3.5. Sulfate Attack Resistance Test

At a steady temperature, mortar prisms of 25 mm × 25 mm × 285 mm were immersed in a solution containing 5% sodium sulfate and magnesium sulfate. This was done in order to assess the resistance of concrete to sulfate attack according to ASTM C1012[38]. In order to evaluate the effects of sulfate-induced expansion, length variations were evaluated on a regular basis. For the purpose of determining the degree of degradation brought on by sulfate-induced chemical processes, mass loss was recorded.

3.6. Chloride Diffusion Test

The ASTM C1556 standard was used in order to ascertain the chloride diffusion coefficient [39]. As seen in Fig. 3, concrete samples were subjected to a solution of 3% sodium chloride for a period of ninety days. Using titration techniques, powdered samples were removed at several depths, and the chloride level was determined using the information obtained. In order to evaluate the impact that SCMs have on the ability to bind chloride, the diffusion coefficient was numerically determined.

3.7. Half-Cell Potential Measurement

An evaluation of the corrosion activity of embedded steel reinforcement was carried out with the help of the half-cell potential test as specified by ASTM C876[40]. On the surface of the concrete, a Cu/CuSO4 electrode that had been saturated was positioned. During the various exposure times, potential readings were monitored and recorded. Voltage readings that were more than -350 mV indicated the presence of active corrosion.

3.8. Linear Polarization Resistance (LPR) Test

An electrochemical workstation was used in order to carry out the LPR test, which was designed to determine the rate of corrosion of steel reinforcement in concrete. After applying a low direct current voltage, the current response that was produced was recorded in order to determine the polarization resistance, which is denoted by the symbol R_p. An increase in the R_p value showed an improvement in corrosion resistance as a result of SCMs and a decrease in permeability.

3.9. Weight Loss Measurement

In order to test the effectiveness of the aggressive sulfate-chloride solution (0.35 M Na_2SO_4 + $MgSO_4$ + NaCl), steel reinforcement bars (rebar) were inserted in concrete and subjected to the solution for a period of ninety days. Following the exposure, the steel bars were taken out, cleaned, and examined for their weight. It was determined how much mass was lost as a result of corrosion.

4. Mix proportions and curing conditions

The concrete mix designs that were used in this investigation were meticulously established in order to evaluate the impact that Supplementary Cementitious Materials (SCMs) have on the durability and corrosion resistance of the concrete. The mix proportions are detailed in Table 10, which includes information on the different degrees of replacement of Ordinary Portland Cement

(OPC) with fly ash (FA), silica fume (SF), ground granulated blast furnace slag (GGBS), and metakaolin (MK).

For the purpose of providing a baseline for comparison, a control mix (CM) was made by using 500 kg/m3 of OPC without any SCM substitution. In the other mixes, various combinations and proportions of SCMs were used, which made it possible to evaluate the impacts of each SCM individually as well as the effects of the combination on the material's strength, permeability, and resistance to corrosion. One example is that M1 through M8 were allowed to undergo standard curing, but M9 through M13 were put through an aggressive sulfate-chloride environment consisting of 0.35 M sodium sulfate, magnesium sulfate, and sodium chloride solution in order to test their tolerance to extreme circumstances. The water-to-binder ratio (w/b) was kept at 0.45, and a superplasticizer dose of 1.5% of the binder weight was employed to improve workability. This was done in particular for high-SCM mixtures, which have a tendency to increase water demand due to the presence of ultrafine particles. It is important to note that M4 and M8 included the largest SCM replacements due to the fact that they replaced up to 75% of OPC.

Table 10: Mix proportions and curing conditions

Mix ID	OPC (kg/m^3)	FA (kg/m^3)	SF (kg/m^3)	GGBS (kg/m^3)	MK (kg/m^3)	Water (kg/m^3)	Superplasticizer (kg/m^3)	Exposure Condition
CM	500	0	0	0	0	225	7.5	Normal Curing
M1	325	50	50	50	25	225	7.5	Normal Curing
M2	275	100	50	50	25	225	7.5	Normal Curing
M3	200	100	50	100	50	225	7.5	Normal Curing
M4	100	150	100	100	50	225	7.5	Normal Curing
M5	375	0	50	50	25	225	7.5	Normal Curing
M6	250	0	100	100	50	225	7.5	Normal Curing
M7	150	0	100	175	75	225	7.5	Normal Curing
M8	100	150	0	175	75	225	7.5	Normal Curing
M9	325	50	50	50	25	225	7.5	0.35 M Na_2SO_4 + $MgSO_4$ + NaCl
M10	200	100	50	100	50	225	7.5	0.35 M Na_2SO_4 + $MgSO_4$ + NaCl
M11	375	0	50	50	25	225	7.5	0.35 M Na_2SO_4 + $MgSO_4$ + NaCl
M12	150	0	100	175	75	225	7.5	0.35 M Na_2SO_4 + $MgSO_4$ + NaCl
M13	100	150	0	175	75	225	7.5	0.35 M Na_2SO_4 + $MgSO_4$ + NaCl

5. Results and Discussions

5.1. Workability

As can be seen in Fig. 4, the slump values varied from 123 mm (M8) to 190 mm (CM), and there was a constant decline in workability as the amount of SCM replacement increased. As a result of the lack of tiny SCM particles, which normally increase surface area and water demand, the control mix (CM) displayed the greatest slump (190 mm), which allowed it to retain a high degree of flowability. On the other hand, mixes that included high levels of SF, GGBS, and MK (M8 and M13) reported the lowest slump values (123–125 mm), which represents a decrease of 35–38% in comparison to CM. In accordance with the results of Chu, and Kwan, [41], who found a slump reduction of 30–40% when these elements were added beyond 15%, the integration of SF and MK had a considerable impact on the workability of the material. It was determined that their ultrafine nature, which brings about an increase in water consumption and paste viscosity, was responsible for the decrease. The use of 1.5% superplasticizer served to successfully preserve enough flowability, ensuring that even high-SCM mixtures remained within acceptable limits for practical applications. This was accomplished in spite of the fact that the workability was reduced. The findings of this study indicate that concerns about workability in heavily substituted mixtures may be alleviated by making the necessary modifications to the admixture.

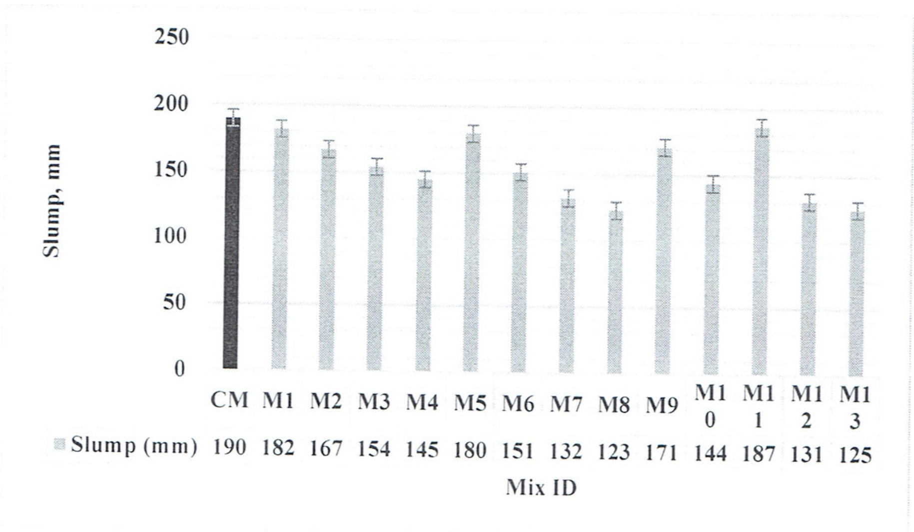

Fig.4. Slump values of various mixes

5.2. Compressive Strength

According to the findings of the development of compressive strength, which are shown in Fig. 5, the SCM-modified mixes demonstrated a considerable improvement in comparison to the control. In order to demonstrate the long-term strength enhancement that is linked with pozzolanic processes and secondary hydration, the CM mix attained 51.2 MPa, whereas M4, M8, and M13 all topped 70 MPa during the course of the experiment. The material with the greatest strength was M13, which had a composition of 30% FA, 20% SF, 35% GGBS, and 15% MK. Its strength was measured at 70.7 MPa. This result was consistent with the results of Miah, et al. [42], who showed that ternary and quaternary SCM mixes developed strength in a manner that was comparable to one another. They made the observation that GGBS contributes to the long-term improvement in strength by densifying the microstructure, while MK boosts early-age strength by speeding hydration processes.

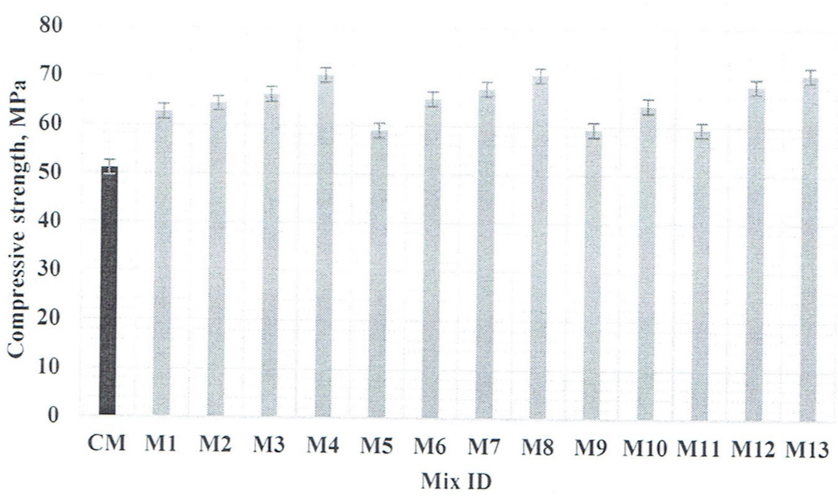

Fig.5. Compressive strength of under normal and aggressive solution exposure

5.3. Water Absorption & Sorptivity

As can be seen in Fig.6, the introduction of SCM resulted in a significant decrease in water absorption and sorptivity. With M8 and M13 obtaining the lowest absorption values (2.3%), this represents a 41% reduction in comparison to CM. In a similar manner, the sorptivity decreased from 0.17 mm/min$^{0.5}$ (CM) to 0.08 mm/min$^{0.5}$ (M8 and M13), which is a 53% improvement. Capillary suction and moisture intrusion are both reduced as a result of these decreases, which imply considerable pore refinement. On the other hand, Mohsen, et al. [43] discovered that a ternary mix of FA, SF, and GGBS decreased sorptivity by more than fifty percent as a result of enhanced particle packing and decreased pore connectivity. This was a pattern that was similar to the one described above. M1–M3, which included modest FA (10–20%), displayed water absorption reductions of just 18–26%, despite the fact that all SCM mixes shown better durability throughout the assessment. It may be inferred from this that in order to achieve maximum pore structure refinement, it is required to have FA replacement levels that are at least thirty percent greater.

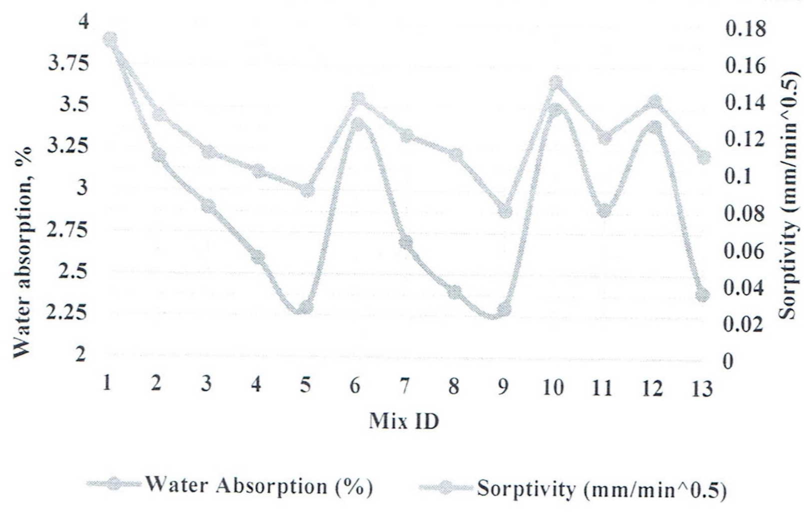

Fig.6. Water absorption and sorptivity of various mixes

5.4. Chloride Permeability & Diffusion

A significant decrease in chloride permeability was seen in mixes that were based on SCM, as shown by the reduced RCPT values that are displayed in Fig. 7. CM measured 3100 Coulombs, which put it in the moderate permeability category according to ASTM C1202 standards. On the other hand, M8 and M13 only managed to accomplish 1000 Coulombs, which is a decrease of 68% and places them in the category of "Very Low Permeability." In a similar manner, chloride diffusion exhibited a decreased trend, with M8 and M13 lowering the diffusion coefficients from 13×10^{-12} m^2/s (CM) to 5×10^{-12} m^2/s (an improvement of 61%). In accordance with the results of Mohseni et al. [44,45], who showed a fifty percent decrease in chloride diffusion with FA and GGBS combinations above fifty percent of total binder content, this validated the function that GGBS and FA play in binding chlorides and limiting ionic transport. Even while M9, M11, and M5 had lesser percentages of SCM, they still demonstrated excellent permeability, with a decrease in RCPT of around 30–40%. This further demonstrates the advantages of even modest amounts of SCM replacement.

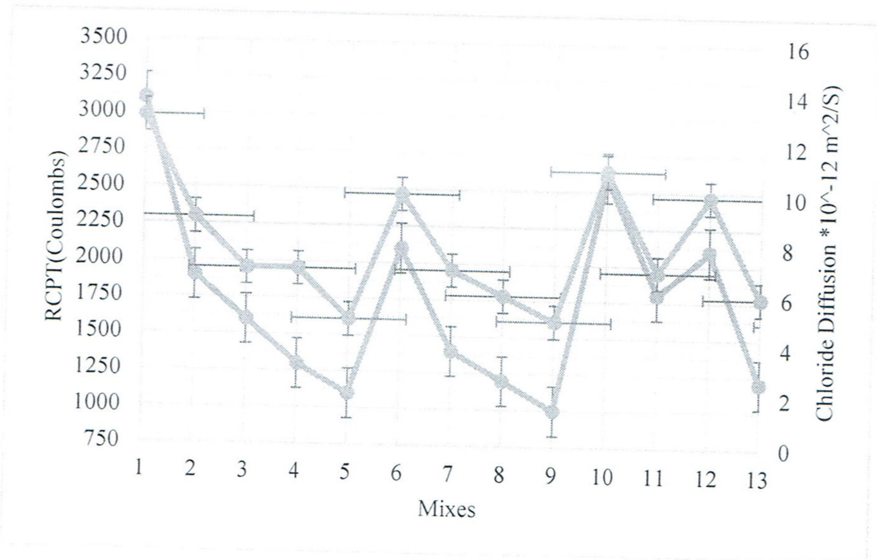

Fig.7. Chloride Permeability & Diffusion of various mixes

5.5. Sulfate Resistance

The introduction of SCM resulted in a considerable reduction in the growth of sulfate, as seen in Fig. 8. The increase of CM was 0.11%, however the expansion of M8 and M13 was just 0.04%, which indicates a 64% decrease in the expansion caused by sulfate. Because GGBS and FA consumed free aluminates, they were able to reduce the amount of ettringite that was formed, which led to an improvement in sulfate resistance. A comparable decrease in sulfate expansion of fifty to seventy percent was recorded by Mehta and Monteiro [46] in SCM-rich concrete, especially when the percentage of GGBS approached thirty percent of the total binder content. Even partial replacement may improve sulfate resistance, as shown by the fact that M6 and M7, which comprised modest quantities of GGBS and FA, displayed a fifty percent decrease in sulfate expansion in comparison to chemical mixture (CM).

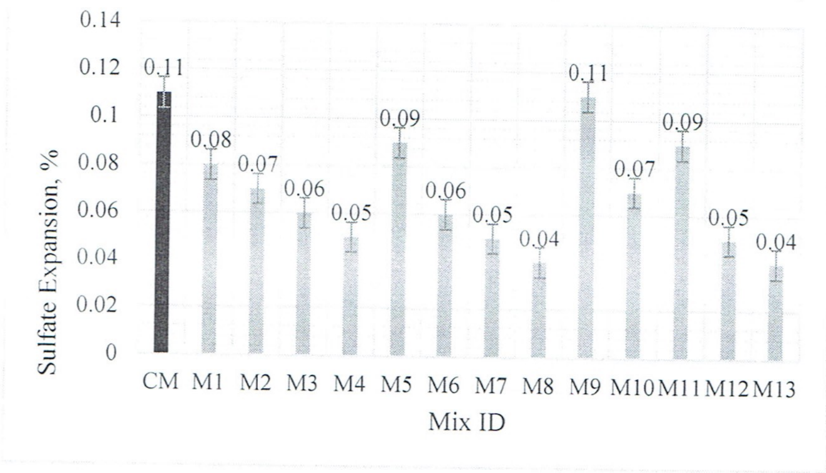

Fig.8. Sulfate reduction of various mixes

5.6. Corrosion Resistance (Half-Cell Potential, LPR, and Weight Loss)

Mixtures that had been changed with SCM had greater corrosion resistance, as shown by increased LPR values and decreased steel weight loss, as shown in Table 11. The results of the half-cell potential significantly improved, going from -293 mV (CM) to -126 mV (M13), which indicates that the danger of active corrosion has decreased. In terms of corrosion resistance, the LPR values went from 10.5 kilo-pascals (CM) to 28.9 kilo-pascals (M8), which is a significant improvement of 175%. The weight loss of steel dropped from 0.83% (CM) to 0.16% (M13), which represents an 81% reduction in the mass loss that was caused by corrosion. According to Chen et al. [47], who found that multi-SCM blends decreased steel corrosion rates by 70–85% owing to enhanced pore structure and chloride binding effects, these results were in agreement with their findings. These three materials, M5, M6, and M10, which had a modest amount of SCM, showed only a 30–45% decrease in corrosion indicators, which further confirms the need for a large amount of SCM in order to provide the highest possible level of reinforcement protection.

Table 11. Results of Corrosion Resistance (Half-Cell Potential, LPR, and Weight Loss) of various mixes

Mix ID	Half-Cell Potential (mV, $Cu/CuSO_4$)	LPR ($k\Omega \cdot cm^2$)	Weight Loss (% of steel mass)
CM	-293	10.5	0.83
M1	-165	22.8	0.55
M2	-157	23.6	0.33
M3	-149	25.5	0.25
M4	-125	26.8	0.17
M5	-174	18.5	0.57
M6	-157	23.7	0.36
M7	-133	26.4	0.26
M8	-127	28.9	0.16
M9	-207	14.6	0.56
M10	-164	20.5	0.34
M11	-178	17.5	0.58
M12	-139	26.7	0.26
M13	-126	28.7	0.16

6. Conclusions

1. The integration of SCMs resulted in a significant improvement in reinforcement protection by lowering the amount of chloride intrusion, sulfate-induced expansion, and steel mass loss. SCM-rich mixtures showed a significant improvement in their half-cell potential, which went from -293 mV (CM) to -126 mV (M13), suggesting a significantly reduced risk of active corrosion. Furthermore, the LPR values shown a remarkable improvement of 175% in corrosion resistance, as they went from 10.5 kilo-pascals (CM) to 28.9 kilo-pascals (M8). Additionally, the reduction in steel weight increased by 81%, going from 0.83% (CM) to only 0.16% (M13).

2. Combinations that had been changed with SCM showed considerable increases in strength, especially in ternary and quaternary mixtures. The control mix (CM) had a compressive strength of 51.2 MPa, while mixes with appropriate SCM concentration had a compressive strength that was more than the 70 MPa threshold. The material with the greatest strength was found to be M13, which measured 70.7 MPa and represented a 38% increase over CM. Pozzolanic reactions of FA and SF were responsible for the increases in strength. These reactions led to an increase in C-S-H formation, a reduction in porosity, and a refined microstructure as a result of the integration of SF and MK and GGBS, which led to an improvement in the development of long-term strength.

3. The use of SCMs improved the material's strength and durability, but they had a detrimental effect on its workability. The slump values dropped from 190 mm (CM) to 123 mm (M8) in formulations that had a high percentage of SF and MK. This represents a reduction of 35–38%. This was anticipated because of the ultrafine particle size of SF and MK, which led to an increase in the need for water. A greater surface area of SCMs, which results in a rise in the viscosity of the paste.

4. Concrete that had been treated with SCM exhibited a considerable decrease in permeability and diffusion rates, which resulted in the material being more resistant to assault from chloride and sulfate. The RCPT stands for the Rapid Chloride Permeability Test. With RCPT values falling from 3100 Coulombs (CM) to 1000 Coulombs (M8, M13), SCM mixes were placed in the "Very Low Permeability" category. This was due to the fact that they lowered chloride permeability by 68%. A drop of 61% was seen in the Chloride Diffusion coefficients, which went from 13×10^{-12} m^2/s (CM) to 5×10^{-12} m^2/s (M8, M13). As expansion values decreased from 0.11% (CM) to 0.04% (M8, M13), sulfate resistance increased by 64% while expansion values remained the same.

5. The performance of tertiary and quaternary SCM combinations was better to that of individual replacements, delivering higher strength, durability, and resistance to corrosion. It was shown that M13, which consisted of 30% FA, 20% SF, 35% GGBS, and 15% MK, had the greatest overall performance across all durability metrics. The M8 strain, which had a high concentration of GGBS and FA, also performed remarkably well, especially in terms of its resistance to chloride and sulfate. Blended systems were more successful than mixes with single SCM replacements (M5, M6, M7), which showed modest improvements but did not approach the performance of blended systems.

References

[1] J.-C. Liu, M. U. Hossain, D. Xuan, H. A. Ali, S. T. Ng, and H. Ye, "Mechanical and durability performance of sustainable concretes containing conventional and emerging supplementary cementitious materials," Developments in the Built Environment, vol. 15, p. 100197, Oct. 2023. https://doi.org/10.1016/j.dibe.2023.100197

[2] B. Kanagaraj, R. Priyanka, N. Anand, T. Kiran, A. D. Andrushia, and E. Lubloy, "A sustainable solution for mitigating environmental corrosion in the construction sector and its socio-economic concern," Case Studies in Construction Materials, vol. 20, p. e03089, Jul. 2024. https://doi.org/10.1016/j.cscm.2024.e03089

[3] A. E. Akinwale, F. V. Adams, and B. D. Ikotun, "Effects of supplementary cementitious materials on concrete reinforcement corrosion in magnesium sulphate," *Materials Today: Proceedings*, vol. 86, pp. 82–87, 2023. https://doi.org/10.1016/j.matpr.2023.03.122

[4] J. Liu, J. Liu, Z. Huang, J. Zhu, W. Liu, and W. Zhang, "Effect of fly ash as cement replacement on chloride diffusion, chloride binding capacity, and micro-properties of concrete in a water soaking environment," *Applied Sciences*, vol. 10, no. 18, p. 6271, 2020. https://doi.org/10.3390/app10186271.

[5] A. M. Tahwia, R. M. Fouda, M. A. Elrahman, and O. Youssf, "Long-term performance of concrete made with different types of cement under severe sulfate exposure," *Materials*, vol. 16, no. 1, p. 240, 2023. https://doi.org/10.3390/ma16010240.

[6] Y. Yuan, K. Niu, B. Tian, L. Li, J. Ji, and Y. Feng, "Effect of metakaolin on the microstructural and chloride ion transport properties of concrete in ocean wave splashing zones," *Materials*, vol. 16, no. 1, p. 7, 2023. https://doi.org/10.3390/ma16010007.

[7] Q. Liang, X. Huang, L. Zhang, and H. Yang, "A review on research progress of corrosion resistance of alkali-activated slag cement concrete," *Materials*, vol. 17, no. 20, p. 5065, 2024. https://doi.org/10.3390/ma17205065.

[8] P. Subpa-asa, N. Nito, S. Fujiwara, and S. Date, "Evaluation of the prediction and durability on the chloride penetration in cementitious materials with blast furnace slag as cement addition," *Construction Materials*, vol. 2, no. 1, pp. 53–69, 2022. https://doi.org/10.3390/constrmater2010005.

[9] Y. F. Silva and S. Delvasto, "Sulfate attack resistance of self-compacting concrete with residue of masonry," *Construction and Building Materials*, vol. 268, p. 121095, Jan. 2021.

[10] P. E. Karthik and V. Gopal, "Carbonation resistance of sustainable concrete with SCMs," *Construction and Building Materials*, vol. 327, p. 126998, 2022. https://doi.org/10.1016/j.conbuildmat.2020.121095

[11] C. Chen, C. Lu, C. Lu, S. Wei, Z. Guo, Q. Zhou, and W. Wang, "Synergetic effect of fly ash and ground-granulated blast slag on improving the chloride permeability and freeze–thaw resistance of recycled aggregate concrete," *Construction and Building Materials*, vol. 365, p. 130015, Feb. 2023. https://doi.org/10.1016/j.conbuildmat.2022.130015

[12] W. V. D. de C. Bezerra, G. R. Meira, and M. S. Freitas, "Combined effect of supplementary cementitious materials and hot-dipped galvanized steel on performance of reinforced concretes subjected to chloride-induced corrosion," *Construction and Building Materials*, vol. 441, p. 137521, Aug. 2024. https://doi.org/10.1016/j.conbuildmat.2024.137521

[13] G. F. Huseien, Z. H. Joudah, N. H. A. Khalid, A. R. M. Sam, M. M. Tahir, N. H. A. S. Lim, R. Alyousef, and J. Mirza, "Durability performance of modified concrete incorporating fly ash and effective microorganism," *Construction and Building Materials*, vol. 267, p. 120947, Jan. 2021. https://doi.org/10.1016/j.conbuildmat.2020.120947

[14] J. Liu, L. Wu, J. Zhu, H. Jia, L. Liu, S. Zhang, C. Yang, Z. Chen, and C. Shi, "Effect of silica fume on corrosion resistance of cement-based materials under carbonic acid water

environment," *Cement and Concrete Composites*, vol. 157, p. 105949, Mar. 2025. https://doi.org/10.1016/j.cemconcomp.2025.105949

[15] C. Bhojaraju, S. S. Mousavi, and C. M. Ouellet-Plamondon, "Influence of GGBFS on corrosion resistance of cementitious composites containing graphene and graphene oxide," *Cement and Concrete Composites*, vol. 135, p. 104836, Jan. 2023. https://doi.org/10.1016/j.cemconcomp.2022.104836

[16] H. Chang, X. Wang, Y. Wang, C. Li, Z. Guo, S. Fan, H. Zhang, and P. Feng, "Chloride binding behavior of cement paste influenced by metakaolin dosage and chloride concentration," *Cement and Concrete Composites*, vol. 135, p. 104821, Jan. 2023. https://doi.org/10.1016/j.cemconcomp.2022.104821

[17] V. Sirivivatnanon, C. Xue, and R. Khatri, "Long-term reinforcement corrosion in low carbon concrete with a high volume of SCMs exposed to NaCl solutions and field marine environment," *Construction and Building Materials*, vol. 393, p. 132071, Aug. 2023.

[18] ASTM C188-22, "Standard Test Method for Density of Hydraulic Cement," ASTM International, 2022. https://doi.org/10.1016/j.conbuildmat.2023.132071

[19] ASTM C204-21, "Standard Test Methods for Fineness of Hydraulic Cement by Air-Permeability Apparatus," ASTM International, 2021.

[20] ASTM C191-20, "Standard Test Methods for Time of Setting of Hydraulic Cement," ASTM International, 2020.

[21] ASTM C109-21, "Standard Test Method for Compressive Strength of Hydraulic Cement Mortars," ASTM International, 2021.

[22] ASTM C114-22, "Standard Test Methods for Chemical Analysis of Hydraulic Cement," ASTM International, 2022.

[23] ASTM C311-21, "Standard Test Methods for Sampling and Testing Fly Ash or Natural Pozzolans," ASTM International, 2021.

[24] ASTM C430-20, "Standard Test Method for Fineness of Hydraulic Cement by the 45-μm (No. 325) Sieve," ASTM International, 2020.

[25] ASTM C618-21, "Standard Specification for Coal Fly Ash and Raw or Calcined Natural Pozzolan," ASTM International, 2021.

[26] ASTM C989-21, "Standard Specification for Ground Granulated Blast-Furnace Slag," ASTM International, 2021.

[27] ASTM C1240-22, "Standard Specification for Silica Fume Used in Cementitious Mixtures," ASTM International, 2022.

[28] ASTM C989-21, "Standard Specification for GGBS in Concrete," ASTM International, 2021.

[29] ASTM C618-21, "Specification for Metakaolin in Concrete," ASTM International, 2021.

[30] ASTM D516-21, "Standard Test Method for Sulfate Ion in Water," ASTM International, 2021.

[31] ASTM C1012-22, "Standard Test Method for Length Change of Hydraulic-Cement Mortars Exposed to a Sulfate Solution," ASTM International, 2022.

[32] ASTM D512-20, "Standard Test Methods for Chloride Ion in Water," ASTM International, 2020.

[33] ASTM C143-21, "Standard Test Method for Slump of Hydraulic-Cement Concrete," ASTM International, 2021.

[34] ASTM C39-22, "Standard Test Method for Compressive Strength of Cylindrical Concrete Specimens," ASTM International, 2022.

[35] ASTM C642-21, "Standard Test Method for Density, Absorption, and Voids in Hardened Concrete," ASTM International, 2021.